Monthly Notices
of the
ROYAL ASTRONOMICAL SOCIETY

MNRAS **503,** L1–L5 (2021) doi:10.1093/mnrasl/slab013

A *Planck*-selected dusty proto-cluster at $z = 2.16$ associated with a strong overdensity of massive Hα-emitting galaxies

Yusei Koyama ,[1,2★] Maria del Carmen Polletta,[3,4] Ichi Tanaka,[1] Tadayuki Kodama,[5] Hervé Dole,[6] Geneviève Soucail,[4] Brenda Frye,[7] Matthew Lehnert[8] and Marco Scodeggio[3]

[1]*Subaru Telescope, National Astronomical Observatory of Japan, 650 North A'ohoku Place, Hilo, HI 96720, USA*
[2]*Graduate University for Advanced Studies (SOKENDAI), Osawa 2-21-1, Mitaka, Tokyo 181-8588, Japan*
[3]*INAF – Istituto di Astrofisica Spaziale e Fisica Cosmica Milano, Via A. Corti 12, 20133 Milano, Italy*
[4]*IRAP, Université de Toulouse, CNRS, CNES, UPS, Toulouse, France*
[5]*Astronomical Institute, Tohoku University, 63 Aramaki, Aoba-ku, Sendai 980-8578, Japan*
[6]*Université Paris–Saclay, CNRS, Institut d'astrophysique spatiale, 91405, Orsay, France*
[7]*Department of Astronomy/Steward Observatory, University of Arizona, 933 N Cherry Ave., Tucson, AZ 85721, USA*
[8]*Sorbonne Université, CNRS UMR 7095, Institut d'Astrophysique de Paris, 98bis bvd Arago, 75014, Paris, France*

Accepted 2021 January 25. Received 2021 January 25; in original form 2020 August 31

ABSTRACT

We have discovered an overdensity of Hα-emitting galaxies associated with a *Planck* compact source in the COSMOS field (PHz G237.0+42.5) through narrow-band imaging observations with the Subaru Multi-Object InfraRed Camera and Spectrograph (MOIRCS). This *Planck*-selected dusty proto-cluster at $z = 2.16$ has 38 Hα emitters including six spectroscopically confirmed galaxies in the observed MOIRCS 4×7 arcmin^2 field (corresponding to $\sim 2.0 \times 3.5$ Mpc^2 in the physical scale). We find that massive Hα emitters with $\log(M_\star/\mathrm{M}_\odot) > 10.5$ are strongly clustered in the core of the proto-cluster (within $\sim$300 kpc from the density peak of the Hα emitters). Most of the Hα emitters in this proto-cluster lie along the star-forming main sequence using Hα-based estimates of the star formation rate (SFR). Meanwhile, the cluster total SFRs derived by integrating the Hα-based SFRs is an order of magnitude smaller than those estimated from *Planck/Herschel* far-infrared photometry. Our results suggest that Hα is a good observable for detecting moderately star-forming galaxies and for tracing the large-scale environment in and around high-redshift dusty proto-clusters. However, there is a possibility that a large fraction of star formation could be obscured by dust and undetected in Hα observations.

Key words: galaxies: clusters: general – galaxies: evolution – galaxies: star formation.

1 INTRODUCTION

Within the framework of hierarchical growth of large-scale structures of the Universe, galaxy clusters evolve at intersections of the cosmic web across cosmic time (e.g. Overzier 2016). Galaxy clusters in the local Universe are dominated by red (quiescent) galaxies with old stellar populations, and they are believed to be formed in the early Universe at $z \gg 1$ accompanying intense starbursts (e.g. Bower, Lucey & Ellis 1992). Young forming clusters are predicted to be observed as strong overdensities of dusty starbursts (Casey 2016; Chiang et al. 2017). Therefore, it is vital to find such star-bursting proto-clusters at high redshift to investigate how the properties of galaxies in today's clusters were put in place.

A growing number of studies have identified such star-forming (or potentially starbursting) proto-cluster candidates in the early Universe using various techniques (e.g. Hayashi et al. 2012; Dannerbauer et al. 2014; Wang et al. 2016; Oteo et al. 2018; Strazzullo et al. 2018; Lacaille et al. 2019). One approach to detect such short-lived (hence rare) dusty objects at high redshift is to use far-infrared (FIR) or (sub)millimetre surveys covering a wide area of the sky. A good example of such dust-selected, highly star-forming systems is the proto-cluster identified around SPT2349–56, the brightest unlensed source from the 2500-deg^2 South Pole Telescope (SPT) survey (Miller et al. 2018; Hill et al. 2020). Here, a large number of submillimetre galaxies (SMGs) at $z = 4.3$ are clustered within a compact region and its total cluster star formation rate (SFR) is estimated to be $\sim 10^4$ M$_\odot$ yr^{-1}.

Planck[1] is a very powerful facility for selecting high-z proto-clusters of dusty sources, taking advantage of its all-sky coverage in the submillimetre range (Clements et al. 2014; Planck Collaboration XXVII 2015; Flores-Cacho et al. 2016; Greenslade et al. 2018; Cheng et al. 2019; Kubo et al. 2019). Using the *Planck* high-z source candidates (PHz) catalogue (Planck Collaboration XXXIX 2016), in combination with *Herschel* photometry (HerMES; Oliver et al. 2012), we investigate the region around a *Planck* source

---

★ E-mail: koyama.yusei@nao.ac.jp

[1] *Planck* is a project of the European Space Agency (ESA) with instruments provided by two scientific consortia funded by ESA member states (in particular, the lead countries France and Italy), with contributions from NASA (USA), and telescope reflectors provided by a collaboration between ESA and a scientific consortium led and funded by Denmark.

Published by Oxford University Press on behalf of Royal Astronomical Society

(PHz G237.0+42.5) lying in the COSMOS field. Within the 4.5-arcmin *Planck* beam (in diameter), there are several *Herschel* FIR sources and X-ray sources. Medium-resolution spectroscopy from follow-up near-infrared Large Binocular Telescope LUCI observations (covering the *Planck* beam area with its 4 × 4 arcmin^2 field of view) and optical Very Large Telescope Visible Multi-Object Spectrograph (VIMOS) spectra from the zCOSMOS survey (Lilly et al. 2007) reveal eight sources at $z = 2.16$ within the *Planck* beam area (Polletta et al., in preparation).

In this letter, we present Hα imaging observations of the PHz G237 field with Subaru Multi-Object InfraRed Camera and Spectrograph (MOIRCS) using a narrow-band (NB) filter (NB2071), which is perfectly matched to the Hα lines from the redshift of this structure ($z = 2.16$). Narrow-band Hα imaging observations are shown to be successful in detecting high-z star-forming galaxies within a narrow redshift slice in various environments (e.g. Geach et al. 2008; Sobral et al. 2013; Tadaki et al. 2013; Hayashi et al. 2016; Darvish et al. 2020). This study presents the first attempt to perform Hα imaging observations towards a *Planck*-selected proto-cluster – with the aim to reveal the structures traced by typical star-forming galaxies, and to study the nature of member galaxies residing in the dust-selected proto-cluster at the peak epoch of galaxy formation. Throughout this letter, we adopt the standard cosmology with $\Omega_{\rm M} = 0.3$, $\Omega_\Lambda = 0.7$ and $H_0 = 70\,{\rm km\,s^{-1}\,Mpc^{-1}}$. All magnitudes are given in the AB system, and we assume the Chabrier (2003) initial mass function (IMF) throughout this work.

2 OBSERVATIONS AND Hα EMITTER SELECTION

We carried out Subaru/MOIRCS observations of the PHz G237 field using the NB2071 filter ($\lambda_{\rm c} = 2.068\ \mu$m, $\Delta\lambda = 0.027\mu$m; corresponding to the Hα line at $z = 2.13$–2.17) on 2018 December 21. The observations were executed in service mode (S18B-206S; PI, Y. Koyama) under very good seeing conditions (FWHM = 0.4 arcsec), and the total exposure time was 180 min. The data are reduced in a standard manner using the MCSRED2 software (Tanaka et al. 2011).

We use $K_{\rm s}$-band images from the UltraVISTA survey with the Visible and Infrared Survey Telescope for Astronomy (VISTA; McCracken et al. 2012) to measure the continuum levels for the NB data. To reliably select emission-line objects, it is important to perform photometry in a consistent way for broad- and narrow-band data. After smoothing our NB image to match the PSF size of the $K_{\rm s}$-band image (0.8 arcsec), we use the dual-image mode of SEXTRACTOR (version 2.19.5; Bertin & Arnouts 1996) to create an NB-selected source catalogue. We use 1.6-arcsec aperture photometry (twice the PSF size in diameter) to determine the source detection and $K_{\rm s}-$NB colours. By distributing apertures (with the same size) at random positions on the NB and $K_{\rm s}$ images, we estimate 5σ limiting magnitudes for NB2071 and $K_{\rm s}$ images as 23.46 and 25.05 mag, respectively. We apply an aperture correction of 0.34-mag to derive their total magnitudes, based on the median difference between the aperture magnitudes (MAG_APER) and Petrosian magnitudes (MAG_AUTO).[2] We detect 829 NB sources (>5σ), in which 800 (97 per cent) sources have counterparts in the COSMOS2015 catalogue (Laigle et al. 2016). We use those 800 galaxies as the parent sample of this study, out of which 142 sources (18 per cent) have redshifts from the COSMOS spectroscopic surveys.

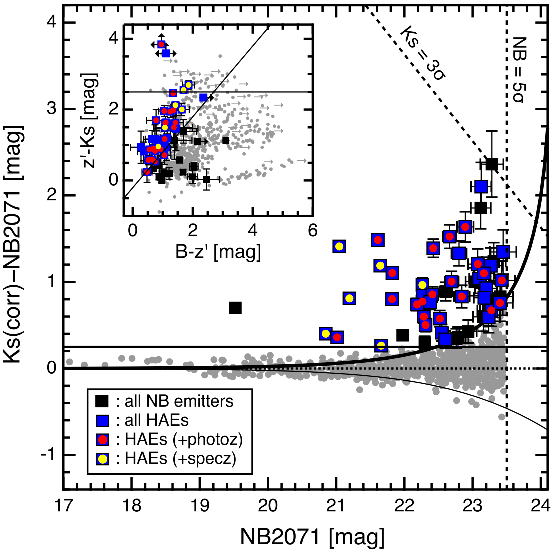

Figure 1. $K_{\rm s}-$NB2071 versus NB2071 magnitudes for all objects in our MOIRCS field (grey dots). The solid curves indicate $\pm 2.5\Sigma$ excess for $K_{\rm s}-$NB colour. The 53 galaxies satisfying $K_{\rm s}-{\rm NB} > 0.25$ (equivalently ${\rm EW}_{\rm rest} > 30$ Å) and $K_{\rm s}-{\rm NB} > 2.5\Sigma$ are defined as NB emitters (black squares). The blue squares are HAEs selected by spec-z (yellow circles), photo-z (red circles) or BzK colours (solid blue squares). In the inset, we show the BzK diagram for all objects, where undetected sources are replaced with their 2σ limits and shown as their upper/lower limits. The solid lines in the inset indicate the original BzK selection determined by Daddi et al. (2004).

In Fig. 1, we plot $K_{\rm s}-$NB colours against their NB magnitudes. Here, we applied a −0.08-mag offset to the $K_{\rm s}$-band magnitudes to account for the spectral slope of the standard star (GD153) used for NB2071 photometry. We also applied a small offset (+0.03 mag) in the NB photometry to set $K_{\rm s}-{\rm NB} = 0$ (median) at the bright end, to properly evaluate the NB excess with respect to the continuum flux density at the same wavelength. We define 53 sources that satisfy $K_{\rm s}-{\rm NB} > 0.25$ and $K_{\rm s}-{\rm NB} > 2.5\Sigma$ as NB emitters (black squares in Fig. 1), where Σ represents the colour excess in $K_{\rm s}-$NB (e.g. Bunker et al. 1995). We note that all the NB emitters identified here are also detected at $\gtrsim 3\sigma$ levels in the UltraVISTA $K_{\rm s}$-band data.

To select Hα emitters (HAEs) at $z = 2.16$ and remove interlopers, we use spectroscopic and photometric redshifts (spec-z and photo-z; from the COSMOS2015 catalogue), and BzK colours. We first select six emitters with $2.150 < z_{\rm spec} < 2.164$ (Polletta et al., in preparation) as spec-z HAEs. For those without spec-z information, we select HAEs using the photo-z ($1.8 < z_{\rm photo} < 2.4$); here, we use ZMINCHI2 from the COSMOS2015 catalogue, defined as the minimum of the χ^2 distribution from the template fitting (see Laigle et al. 2016 for details). In addition, we select NB emitters satisfying the BzK criteria (Fig. 1), regardless of their photo-z. Because the photo-z uncertainty is often large for star-forming galaxies with blue/featureless spectral energy distributions (SEDs) at $z \sim 2$, the BzK selection combined with the NB excess is shown to be an efficient way for selecting HAEs at the targeted redshifts (e.g. Koyama et al. 2013a; Shimakawa et al. 2018). Amongst the 53 NB emitters, we select 38 HAEs in total: six galaxies as spec-z HAEs, 25 galaxies as photo-z HAEs (five of which are spec-z HAEs) and 12 additional galaxies as BzK HAEs. As can be seen in the BzK diagram, most of the spec-z and photo-z HAEs also satisfy BzK selection. We note that three NB emitters are not

---

[2] Three Hα emitters selected in this study do not satisfy $K_s-{\rm NB} > 0.25$ if we use MAG_AUTO to define an NB excess. The cluster total Hα SFR would be reduced by ∼12 per cent if we removed these sources from the analyses.

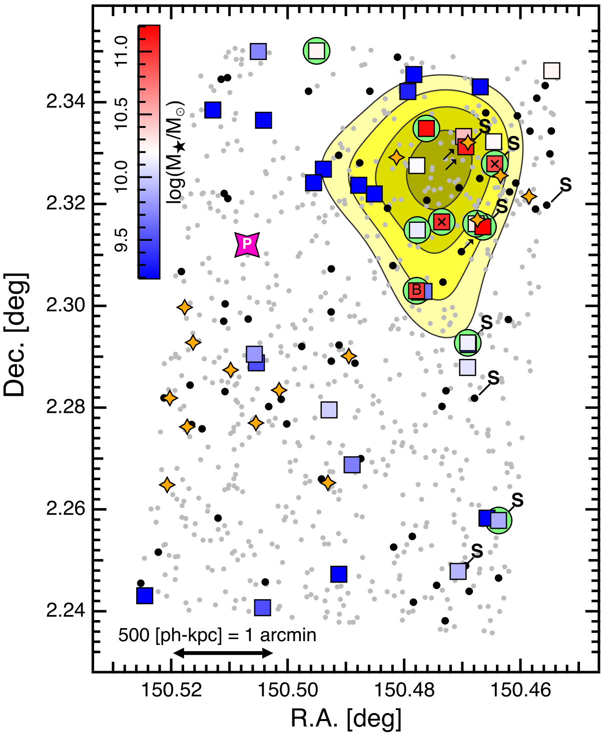

Figure 2. The two-dimensional sky distribution of HAEs (coloured squares), with the colour code indicating their $M_\star$. The grey circles show all NB sources, out of which black circles indicate galaxies with $1.8 < z_{\rm photo} < 2.4$. The green circles are HAEs detected at 24 μm. Two sources marked with '×' are X-ray detected HAEs, and eight sources marked with 'S' are spectroscopic members. Three arrows indicate HAEs that do not satisfy $K_s - {\rm NB} > 0.25$ when we use MAG_AUTO, and one source marked with 'B' shows the HAE that is undetected in both the B and z' bands. To guide the eye, the yellow-shaded contours indicate 1.5σ, 2.0σ, 2.5σ and 3.0σ above the median local number density measured with HAEs. The orange stars show the red *Herschel* sources (see Section 3.3). The coordinates of the *Planck* source (RA, Dec.) = (150.507, +2.31204) are shown by the pink star marked with 'P'.

detected at the B or z' band, one of which is undetected at both the B and z' bands. We keep these sources because their lower/upper limits still satisfy the BzK criteria. We note that the source undetected at both the B and z' bands is indicated by a 'B' in Fig. 2, and this source contributes 4.5 per cent of the cluster total SFR.

3 RESULTS AND DISCUSSION

3.1 Massive Hα emitters in the proto-cluster core

We show in Fig. 2 the two-dimensional distribution of the HAEs (squares), photo-z selected potential cluster members ($1.8 \le z_{\rm photo} \le 2.4$; black circles) and all the NB-detected objects (grey circles) in the PHz G237 field. Objects marked with 'S' are spectroscopic members, six of which are HAEs. We compute the local number density of HAEs at a given point by applying Gaussian smoothing ($\sigma = 300$ kpc) for each HAE and by combining the tails of those Gaussian wings (see contours in Fig. 2). The smoothing radius is chosen following the typical size of HAE overdensities associated with rich proto-clusters at similar redshifts (e.g. Koyama et al. 2013a). We determine (RA, Dec.) = (10:01:53.67, +02:19:38.9) as the HAE density peak.

In Fig. 2, HAE symbols are colour-coded based on their $M_\star$ (i.e. redder colours indicate higher $M_\star$). Stellar masses of HAEs are derived by fitting the SEDs (*uBVrizJHK* and IRAC ch1 and ch2 photometry from COSMOS), using the FAST code (Kriek et al. 2009). We assume a fixed redshift ($z = 2.16$), the Bruzual & Charlot (2003) stellar population synthesis model, the Calzetti et al. (2000) dust attenuation law and the Chabrier (2003) IMF. We also assume exponentially declining SFRs, SFR $\propto \exp(-t/\tau)$, with parameter ranges of τ and age of 10^7–10^{10} yr, metallicity = [0.004, 0.008, 0.02] and $A_V = 0.0$–3.0 mag.

Fig. 2 demonstrates that massive HAEs (with $M_\star \gtrsim 10^{10.5}\,{\rm M}_\odot$) are strongly clustered around the density peak. A similar trend was reported for other candidate proto-clusters at $z \gtrsim 2$ (e.g. Hatch et al. 2011; Matsuda et al. 2011; Koyama et al. 2013a), suggesting an accelerated galaxy growth in dense environments in the early Universe. We note that many of those massive HAEs residing in the proto-cluster environment are individually detected in the Multiband Imaging Photometer for *Spitzer* (MIPS) 24-μm image (as shown by green circles in Fig. 2). Their stellar masses are already comparable with present-day massive cluster galaxies, but they are still actively forming stars (see also Section 3.2). It should also be noted that two of the massive HAEs near the density peak are X-ray sources (see the '×' marks in Fig. 2), suggesting that the Hα emission of these two galaxies may be contributed by active galactic nuclei (AGNs). The stellar masses of these X-ray HAEs may be overestimated, but their stellar masses would still be higher than the median $M_\star$ of our HAE sample, even if we consider a significant fraction of their $M_\star$ estimates to be contributed by AGNs (see Section 3.2).

3.2 Proto-cluster HAEs on the SFR–$M_\star$ relation

We derive the Hα+[N II] line fluxes ($F_{{\rm H}\alpha+[{\rm N\,II}]}$), continuum flux density ($f_{\rm c}$), and the rest-frame equivalent widths (EW$_{\rm rest}$) of HAEs from the K_s band and NB2071 photometry in the same way as Koyama et al. (2013a). We estimate the contribution of [N II] lines ([N II]/Hα ratio) and Hα dust attenuation ($A_{{\rm H}\alpha}$) using the empirical calibrations established for local star-forming galaxies; we use the [N II]/Hα–EW$_{\rm rest}$(Hα) relation presented by Sobral et al. (2012), and the $A_{{\rm H}\alpha}$–$M_\star$–EW$_{\rm rest}$(Hα) relation from Koyama et al. (2015).[3] We then convert the Hα luminosity to SFR$_{{\rm H}\alpha}$ using the Kennicutt (1998) relation by taking into account the IMF difference.

In Fig. 3, we show the SFR–$M_\star$ diagram for the HAEs in the PHz G237 field (coloured symbols). In this plot, the colour-coding indicates the distance from the HAE density peak; the redder colour symbols show HAEs located closer to the highest-density region. It can be seen that the $M_\star$ distribution of HAEs near the density peak (red/orange symbols) tend to be skewed to the massive end, as already discussed in Section 3.1. We also plot in Fig. 3 the HAEs in the Spiderweb proto-cluster at the same redshift ($z = 2.16$) selected using the same NB filter and the same instrument (Shimakawa et al. 2018; see also Koyama et al. 2013a). For HAEs with $\log(M_\star/{\rm M}_\odot) > 9.5$, we find that the fraction of massive HAEs (with $\log(M_\star/{\rm M}_\odot) > 10.5$) is consistent between PHz G237 (26 ± 12 per cent) and Spiderweb (30 ± 9 per cent). The dot-dashed line in Fig. 3 is the star formation main sequence (SFMS) derived for the field HAEs at $z \sim 2$ (Oteo et al. 2015). We note that all these studies are based on HAEs,

---

[3] We confirmed that our conclusions are unchanged even if we use A_V derived from SED fitting to predict $A_{{\rm H}\alpha}$, assuming the Calzetti et al. (2000) curve and $E(B-V)_{\rm star}/E(B-V)_{\rm gas} = 0.44$. We find that the average dust-corrected SFRs could be higher by a factor of ∼1.8× in this case, but we caution that there is a large uncertainty in the $E(B-V)_{\rm star}/E(B-V)_{\rm gas}$ ratio (which can be 0.44–1.0; see, e.g., Koyama et al. 2019).

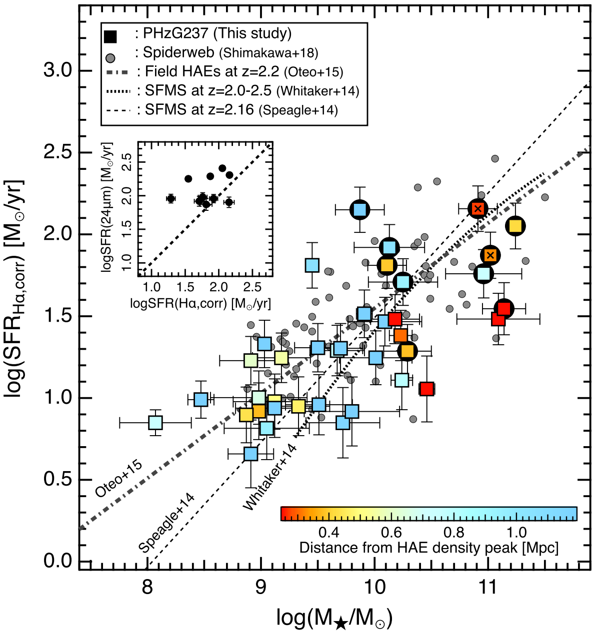

Figure 3. SFR–$M_\star$ diagram for HAEs in the PHz G237 proto-cluster field (squares). The colour-coding indicates the distance from the HAE density peak. The large black circles show HAEs detected at 24 μm, and the '×' marks indicate X-ray sources. We also show HAEs in the Spiderweb proto-cluster at the same redshift from Shimakawa et al. (2018), and the dot-dashed line indicates the SFR–$M_\star$ relation for HAEs in the field environment at $z \sim 2$ (Oteo et al. 2015). For comparison, we also show the SFMS at $z \sim 2$ defined by Speagle et al. (2014) and Whitaker et al. (2014). In the inset, we compare the SFRs derived from Hα and 24-μm fluxes for HAEs detected at 24 μm.

and we use similar approaches to derive $M_\star$ and SFRs. Our results suggest that the SFMS for HAEs in the PHz G237 proto-cluster field is broadly consistent with that in the Spiderweb proto-cluster and in the general field at similar redshifts. This suggests similar mass growth rates in all environments at a given stellar mass, consistent with our previous studies (e.g. Koyama et al. 2013b).

The two X-ray detected HAEs are shown with '×' marks in Fig. 3. If we remove these two AGN candidates, massive HAEs within ~500 kpc from the density peak tend to be located below the SFMS. This result may suggest a decline of specific SFRs in dense environments. However, we must wait for future spectroscopic observations because accurate dust attenuation correction is critical to reliably measure the SFRs of such massive star-forming galaxies at high-z. In fact, there are two HAEs detected at 24 μm that are located significantly below the SFMS in Fig. 3. However, their SFRs that are derived from 24-μm photometry (using the SED templates presented by Wuyts et al. 2008) turn out to be ~0.6–0.7 dex higher than we expected from the dust-corrected Hα line (see the inset in Fig. 3). Unfortunately, the IR-based SFRs are not available for other MIPS-undetected HAEs (and SFRs from 24 μm alone also suffer from large uncertainties). In any case, we need spectroscopic follow-up observations to accurately measure the dust attenuation effects, in order to discuss the exact locations of proto-cluster HAEs with respect to the SFMS.

3.3 Cluster total SFR from Hα and IR

In Fig. 4, we show the cumulative SFR distribution from the HAE density peak (out to 1 Mpc). The black and grey lines represent the results when we use dust-corrected and dust-uncorrected Hα SFRs, respectively. For both black and grey lines, the solid lines show the results for all HAEs, while the dashed lines show the results when we remove two X-ray AGNs. We also show in Fig. 4 the cluster-integrated SFRs measured with various approaches. The blue hatched region shows the integrated dust-corrected SFR$_{\mathrm{H}\alpha}$ for all HAEs within the MOIRCS field of view (the width of the hatched region indicates the results with/without AGNs). The orange shaded region shows the integrated SFR(MIR)s of the HAEs detected at 24 μm. It seems that the total dust-corrected SFR$_{\mathrm{H}\alpha}$ is consistent with the 24 μm based SFR, but we caution that the total MIPS SFR is computed only for 10 HAEs that individually detected at 24μm, and thus can be regarded as the lower limit for the cluster total SFR.

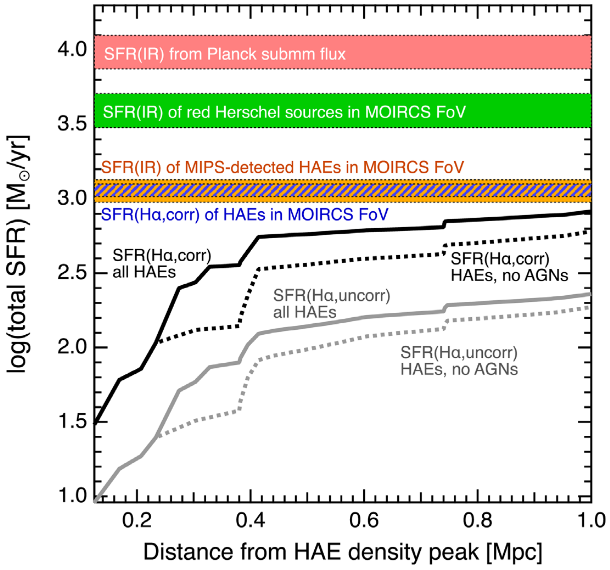

Figure 4. Cluster-integrated (cumulative) SFRs for HAEs in the PHz G237 proto-cluster field plotted against the distance from the HAE density peak. The black/grey lines show the results for the Hα-based SFRs with/without dust attenuation correction. In both cases, solid lines are the results for all HAEs, while the dashed lines are the results for non-AGN HAEs by removing two X-ray sources. We also show the cluster total SFRs measured with various methods. The blue hatched area shows the total dust-corrected SFR(Hα)s for all 38 HAEs within the MOIRCS field of view, while the orange shaded region shows the sum of the IR-derived SFRs for HAEs detected at 24 μm in the same field of view (the widths of the stripes indicate the results with/without the AGN effects). We also show the FIR-derived total SFR measured from *Planck* submillimetre flux (red shaded region) and from FIR sources with red *Herschel* colours located within the MOIRCS field of view (green shaded region).

The green shaded region in Fig. 4 shows the cluster total SFR$_{\mathrm{FIR}}$ as a sum of 15 *Herschel* sources with red FIR colours ($S_{350}/S_{250} > 0.7$ and $S_{500}/S_{350} > 0.6$; Planck Collaboration XXVII 2015) in the MOIRCS field of view (see orange stars in Fig. 2). Here we use the CMCIRSED package (Casey 2012) to fit the *Herschel*/SPIRE photometry with a modified grey-body function at $T_{\mathrm{dust}} = 30$ K and $T_{\mathrm{dust}} = 35$ K (with fixed $\beta = 1.8$) to estimate the total L_{IR}(8–1000 μm). The FIR colour criteria are supposed to select galaxies at $z \sim 2$–4 (and may suffer from foreground/background interlopers), but it is worth noting that the total SFR could be ~5 times higher than we expect from Hα. We also calculate the SFR(FIR) from the *Planck* 857-GHz and 545-GHz fluxes (assuming $z = 2.16$ and $T_{\mathrm{dust}} = 30$ K; the red shaded region in Fig. 4). We must regard this as an upper limit of the cluster total SFR as the *Planck* fluxes are contributed by all sources within the *Planck* beam (see consistent results in Planck

Collaboration XXVII 2015). We also note that our Hα data do not cover the full *Planck* beam area (see Fig. 2). In addition, some sources may lie outside the redshift range covered by the NB filter ($\Delta v \gtrsim 2000$ km s^{-1}). Therefore, we cannot rule out the possibility that there exist other structures contributing to the *Planck* fluxes outside the current Hα survey.

Our results suggest that the cluster total SFR measured with Hα could be an order of magnitude smaller than IR-based SFRs. This large difference may in part come from uncertainties in calibration between Hα- and IR-based SFRs at high-z, or we may underestimate the Hα dust attenuation for individual HAEs. It is also possible that a large number of cluster members that are not identified as HAEs contribute to the cluster total IR luminosities (such as 'optically dark' galaxies; e.g. Simpson et al. 2014; Franco et al. 2018). Deep and wide-field submillimetre mapping with ALMA (e.g. Umehata et al. 2017; Kneissl et al. 2019) would be a powerful approach to resolve the dust-enshrouded star-forming activity within young dusty proto-clusters.

4 SUMMARY

With our Subaru/MOIRCS NB Hα imaging observations towards a *Planck* compact source lying in the COSMOS field (PHz G237.0+42.5), we report the discovery of a dusty proto-cluster at $z = 2.16$ associated with an overdensity of massive HAEs. We identified 38 HAEs at $z = 2.16$ within the observed 4×7 arcmin^2 field of view, out of which six galaxies are spectroscopically confirmed. We find that massive HAEs (with $M_\star > 10^{10.5}\,\mathrm{M}_\odot$) are strongly clustered in the proto-cluster core region (within ~300 kpc from the HAE density peak). Most of the HAEs in the PHz G237 proto-cluster region are typical star-forming galaxies on the SFMS. While we find that the most massive HAEs may have suppressed SFRs (from Hα-based SFR estimates), their 24 μm derived SFRs are consistent with lying along the SFMS. By integrating the Hα-based SFRs of all HAEs, we estimate that the cluster total Hα SFR could be an order of magnitude smaller than that predicted from *Planck/Herschel* FIR photometry. Our results suggest that Hα is a good indicator for detecting moderately star-forming galaxies and tracing the large-scale environment in and around high-z dusty clusters. However, there remains a possibility that a significant amount of star formation is obscured by dust and is unseen by Hα observations.

ACKNOWLEDGEMENTS

We thank the reviewer for a careful reading and constructive comments, which improved the paper. The narrow-band imaging data used in this paper are collected at the Subaru Telescope, which is operated by the National Astronomical Observatory of Japan (NAOJ). This work was financially supported in part by a Grant-in-Aid for the Scientific Research (No. 18K13588) by the Japanese Ministry of Education, Culture, Sports and Science. MP acknowledges financial support from Labex OCEVU. This research has made use of data from the HerMES project (http://hermes.sussex.ac.uk/).

DATA AVAILABILITY

The data underlying this article will be shared on reasonable request to the corresponding author.

REFERENCES

Bertin E., Arnouts S., 1996, A&AS, 117, 393
Bower R. G., Lucey J. R., Ellis R. S., 1992, MNRAS, 254, 601
Bruzual G., Charlot S., 2003, MNRAS, 344, 1000
Bunker A. J., Warren S. J., Hewett P. C., Clements D. L., 1995, MNRAS, 273, 513
Calzetti D., Armus L., Bohlin R. C., Kinney A. L., Koornneef J., Storchi-Bergmann T., 2000, ApJ, 533, 682
Casey C. M., 2012, MNRAS, 425, 3094
Casey C. M., 2016, ApJ, 824, 36
Chabrier G., 2003, PASP, 115, 763
Cheng T. et al., 2019, MNRAS, 490, 3840
Chiang Y-K., Overzier R. A., Gebhardt K., Henriques B., 2017, ApJ, 844, L23
Clements D. L. et al., 2014, MNRAS, 439, 1193
Daddi E. et al., 2004, ApJ, 617, 746
Dannerbauer H. et al., 2014, A&A, 570, A55
Darvish B. et al., 2020, ApJ, 892, 8
Flores-Cacho I. et al., 2016, A&A, 585, A54
Franco M. et al., 2018, A&A, 620, A152
Geach J. E., Smail I., Best P. N., Kurk J., Casali M., Ivison R. J., Coppin K., 2008, MNRAS, 388, 1473
Greenslade J. et al., 2018, MNRAS, 476, 3336
Hatch N. A., Kurk J. D., Pentericci L., Venemans B. P., Kuiper E., Miley G. K., Röttgering H. J. A., 2011, MNRAS, 415, 2993
Hayashi M., Kodama T., Tadaki K-i., Koyama Y., Tanaka I., 2012, ApJ, 757, 15
Hayashi M. et al., 2016, ApJ, 826, L28
Hill R. et al., 2020, MNRAS, 495, 3124
Kennicutt R. C., 1998, ApJ, 498, 541
Kneissl R. et al., 2019, A&A, 625, A96
Koyama Y. et al., 2013a, MNRAS, 428, 1551
Koyama Y. et al., 2013b, MNRAS, 434, 423
Koyama Y. et al., 2015, MNRAS, 453, 879
Koyama Y., Shimakawa R., Yamamura I., Kodama T., Hayashi M., 2019, PASJ, 71, 8
Kriek M., van Dokkum P. G., Labbé I., Franx M., Illingworth G. D., Marchesini D., Quadri R. F., 2009, ApJ, 700, 221
Kubo M. et al., 2019, ApJ, 887, 214
Lacaille K. M. et al., 2019, MNRAS, 488, 1790
Laigle C. et al., 2016, ApJS, 224, 24
Lilly S. J. et al., 2007, ApJS, 172, 70
Matsuda Y. et al., 2011, MNRAS, 416, 2041
McCracken H. J. et al., 2012, A&A, 544, A156
Miller T. B. et al., 2018, Nature, 556, 469
Oliver S. J. et al., 2012, MNRAS, 424, 1614
Oteo I. et al., 2018, ApJ, 856, 72
Oteo I., Sobral D., Ivison R. J., Smail I., Best P. N., Cepa J., Pérez-García A. M., 2015, MNRAS, 452, 2018
Overzier R. A., 2016, A&ARv, 24, 14
Planck Collaboration et al., 2015, A&A, 582, A30
Planck CollaborationXXXIX, 2016, A&A, 596, A100
Shimakawa R. et al., 2018, MNRAS, 481, 5630
Simpson J. M. et al., 2014, ApJ, 788, 125
Sobral D. et al., 2013, MNRAS, 428, 1128
Sobral D., Best P. N., Matsuda Y., Smail I., Geach J. E., Cirasuolo M., 2012, MNRAS, 420, 1926
Speagle J. S., Steinhardt C. L., Capak P. L., Silverman J. D., 2014, ApJS, 214, 15
Strazzullo V. et al., 2018, ApJ, 862, 64
Tadaki K., Kodama T., Tanaka I., Hayashi M., Koyama Y., Shimakawa R., 2013, ApJ, 778, 114
Tanaka I. et al., 2011, PASJ, 63, 415
Umehata H. et al., 2017, ApJ, 835, 98
Wang T. et al., 2016, ApJ, 828, 56
Whitaker K. E. et al., 2014, ApJ, 795, 104
Wuyts S., Labbé I., Förster Schreiber N. M., Franx M., Rudnick G., Brammer G. B., van Dokkum P. G., 2008, ApJ, 682, 985

This paper has been typeset from a TEX/LATEX file prepared by the author.